Published in final edited form as:
J Mater Chem B Mater Biol Med. 2014 November 14; 2(42): 7316–7326. doi:10.1039/C4TB01084A.

Synthesis and Self-Assembly of a Mikto-Arm Star Dual Drug Amphiphile Containing both Paclitaxel and Camptothecin

A.G. Cheetham[a,b], **P. Zhang**[a], **Y.-A. Lin**[a,b], **R. Lin**[a], and **H. Cui**[a,b]

H. Cui: hcui6@jhu.edu

[a]Department of Chemical and Biomolecular Engineering, The Johns Hopkins University, Baltimore, Maryland 21218, USA

[b]Institute for NanoBioTechnology, The Johns Hopkins University, Baltimore, Maryland 21218, USA

Abstract

Self-assembly of anticancer therapeutics into discrete nanostructures provides an innovative way to develop a self-delivering nanomedicine with a high, quantitative drug loading. We report here the synthesis and assembly of a mikto-arm star dual drug amphiphile (DA) containing both a bulky paclitaxel (PTX) and a planar camptothecin (CPT). The two anti-cancer drugs of interest were stochastically conjugated to a β-sheet forming peptide (Sup35) and under physiologically-relevant conditions the dual DA could spontaneously associate into supramolecular filaments with a fixed 41% total drug loading (29% PTX and 12% CPT). Transmission electron microscopy imaging and circular dichroism spectroscopy studies reveal that the bulkiness of the PTX, as well as the π-π interaction preference between the CPT units, has a significant impact on the assembly kinetics, molecular level packing, and nanostructure morphology and stability. We found that the DA containing two PTX units assembled into non-filamentous micelle-like structures, in contrast to the filamentous structures formed by the hetero dual DA and the DA containing two CPTs. The hetero dual DA was found to effectively release the two anticancer agents, exhibiting superior cytotoxicity against PTX-resistant cervical cancer cells. The presented work offers a potential method to generate well-defined entwined filamentous nanostructures and provides the basis for a future combination therapy platform.

Introduction

Since the advent of Supramolecular Chemistry, the self-assembly of small molecules into discrete nanostructures has rapidly become a valuable tool for the creation of functional materials.[1, 2] Through the spontaneous association of appropriately designed monomers, nano-sized entities can be constructed that possess a well-defined shape and distinct physicochemical properties. The morphology of these assembled structures is determined by the constituent parts of the monomer, which by necessity is often amphiphilic in nature and therefore composed of hydrophilic and hydrophobic domains. These building blocks vary widely in their properties, offering a multitude of options for directing the assembly toward

a particular nanostructure. Hydrophilic segments, for example, range from simple charged (phosphate,[3] ammonium,[4–6] carboxylate[7]) and neutral (oligo-ethylene glycol,[8,9] oligo-saccharides[10]) groups to more complex oligo-peptides, [11–18] and peptide nucleic acids.[19] Hydrophobic segments include linear hydrocarbons, and simple[20] and extended[3, 8, 21, 22] aromatic systems.

A promising application of this molecular assembly approach is for the creation of biologically active materials,[23–27] with the delivery of therapeutic agents being a particular avenue of development. Molecular assembly of anticancer prodrugs into nanostructures is an emerging area in the drug delivery field due to the potential advantages it offers over methods that rely on encapsulation within or conjugation to polymers or other nano-objects.[28–31] By incorporating a drug molecule as one component of an amphiphilic monomer, the drug becomes part of its own delivery vehicle—a nano-sized entity that possess a well-defined shape and distinct physicochemical properties different to those of the drug. This approach offers much greater control over the drug loading and eliminates any loading polydispersity among individual nanostructures. For example, work by the groups of Couvreur[32] and Jin,[33] who both conjugated lipid-like moieties to hydrophilic drugs, gave rise to nano-sized assemblies through spontaneous self-association. These self-assembled drug delivery systems were later complemented by Shen *et al*,[34] who grafted a hydrophilic tail to a hydrophobic drug to form spherical nanostructures.

Further advances in this field have led to formation of a variety of interesting assembled nanostructures, such as micelles,[35, 36] filaments,[37–39] and hydrogels,[38, 40, 41] through the incorporation of additional molecular elements into the amphiphilic prodrug that can be used to influence the structure of the final assembly. Xu and co-workers have utilized this approach to create hydrogel-forming amphiphilic prodrugs,[40] while our own lab has created filamentous assemblies with well-defined nanostructures (drug amphiphiles).[37–39, 42] Yang and co-workers have also demonstrated a peptide-based molecular hydrogelator that contains both an anti-inflammatory agent and an anticancer drug, exhibiting effective cytotoxicity against the Hep G2 cell line. The development of self-assembled drug delivery systems containing two or more different drugs is important as combination therapy is commonly used to help improve treatment efficacy and reduce the likelihood of multidrug resistance (MDR).[43] Being able to deliver two drugs to the same site simultaneously may enable benefits that while seen *in vitro* do not necessarily translate to the clinic due to the differing pharmacokinetic properties of the two drugs.

Understanding how the self-assembly of self-assembled drug delivery systems containing two different drug molecules is necessary if effective materials are to be created, but as yet little is known concerning the interplay between the molecular structure and nanostructure and how this subsequently affects the physicochemical properties for even single drug-containing self-assembled drug delivery systems. For example, Chilkoti and co-workers reported that the self-assembly behaviour of drug–polypeptide conjugates can be tuned through the Log D value (a measure of hydrophobicity) of the drug.[44] We found that the nanostructure can influence the drug release properties in unexpected ways, promoting formation of prodrug dimers that prevented the rapid release of the active drug.[37] What is clear is that though the morphology of these assembled structures is mostly determined by

the intermolecular interactions between monomers, the physical packing at the molecular level within the assembly must not be overlooked as this too can strongly influence the nanostructure morphology[45–50] and the emergent physicochemical properties.[50–54]

We recently reported the synthesis of a mikto-arm star peptide amphiphile in which two *chemically* distinct entities, a hydrocarbon and a fluorocarbon, were incorporated into the same molecule. This gave rise to interesting self-assembly characteristics through the molecular frustration introduced by their mutual immiscibility.[55] To our knowledge, there are no examples that utilize two *structurally* distinct entities as the hydrophobic block of a single amphiphilic molecule and we speculate that this may also be a promising and effective strategy to influence the self-assembly process as a result of their differing packing preferences.

Herein, we use this strategy to create a dual drug amphiphile (DA) that contains both camptothecin (CPT) and paclitaxel (PTX), using our mikto-arm star platform as a scaffold. These two anticancer drugs not only exert cytotoxicity via differing mechanisms, but also possess very different molecular structures. We found that the CPT- and PTX-containing dual DA could indeed self-assemble into well-defined nanostructures, but that the final morphology and assembly pathway were both significantly altered with respect to a dual CPT-containing DA. The observed differences clearly result from the bulky nature of PTX, as the dual PTX-containing DA formed only small non-filamentous structures.

Results and Discussion

Dual Drug Amphiphile Design and Synthesis

Incorporating two different drug molecules into a single self-assembling entity presents a challenge when the overall properties of the conjugate are expected to depend strongly on the nature of those drugs. We chose to investigate the combination of CPT and PTX as these are two effective anti-neoplastic agents that possess very different molecular structures (Fig. 1a) and mechanisms of action. CPT, a DNA topoisomerase I inhibitor,[56] is a planar aromatic molecule that aggregates through face-to-face π–π interactions.[57] In contrast, the mitotic inhibitor PTX[58] is a very bulky, three-dimensional molecule that undergoes self-aggregation through hydrogen bond formation.[59] Whilst their use in combination has been limited, being shown to be non-interactive at best,[60] in the context of self-assembly they serve an important purpose for exploring how two disparate building blocks can affect the overall assembly process and nanostructure morphology. Given our focus here is to study the effect that incorporating the two drugs has on self-assembly, we opted to simply use the same linker—the reducible disulfylbutyrate linker[61]—to conjugate both drugs to the hydrophilic peptide, rather than linkers that would allow attachment via orthogonal reaction mechanisms. The latter approach is certainly possible, however, and would open up the possibility of differential drug release through separate degradation pathways. The β-sheet forming peptide was chosen to be a sequence derived from the Sup35 yeast prion,[62] $GN_2Q_2NYK_2$, with the two added lysine residues providing a charged head group and the glycine acting as a spacer. This sequence contains more hydrophilic residues than the Tau sequence we have previously utilized,[38, 39] and is expected to provide greater solubility to the final conjugate, **CPT-PTX-Sup35**. Conjugation of the two drugs can be accomplished

using directed disulphide formation, requiring the incorporation of two thiol-containing cysteine residues into the peptide. The total drug loading of this conjugate is fixed at 41%, with a CPT and PTX content of 12 and 29%, respectively (see S1.4 in the ESI†).

The dual DA, **CPT-PTX-Sup35**, was synthesized by statistical reaction with a 1:1 mixture of the activated drugs, **CPT-buSS-Pyr** and **PTX-buSS-Pyr**, in nitrogen-purged DMSO (Fig. 1b). Given the significant difference in structure between the two drugs, it was expected that there would be a subsequent difference in the product distribution, particularly with regard to the addition of the second drug. To probe this, **dCys-Sup35** was reacted with one equivalent per thiol of the 1:1 drug mixture, purifying the reaction by reversed-phase HPLC before it had reached completion (Fig. 1c). The resulting drug-containing species were isolated and calibrated in order to determine the absolute amounts of each conjugate formed. We found that the singly reacted species, **CPT-Cys-Sup35** and **PTX-Cys-Sup35**, were formed in similar proportions (39 and 33% respectively), with each giving the two expected positional isomers, as indicated by the occurrence of two closely separated peaks for each species. These species were found to have reactive thiol groups (Figs. S5 and S6 in ESI†), which upon dissolution in PBS were observed to form scrambled products through disulphide exchange. The remaining products of the reaction were found to be the hetero-dual DA, **CPT-PTX-Sup35**, and the two homo-dual DAs, **dCPT-Sup35** and **dPTX-Sup35**. The product distribution was observed to be biased towards the less sterically crowded **dCPT-Sup35**, with only 6% each of the two PTX-containing conjugates. Reaction of **PTX-Cys-Sup35** with either of the two activated drugs may be hindered due to the bulky PTX, potentially causing similar issues for the reaction of **CPT-Cys-Sup35** with **PTX-buSS-Pyr**.

In order to push the reaction towards completion, **dCys-Sup35** was allowed to react with a three-fold excess per thiol of the 1:1 activated drug mixture for 5 days (Fig. 1d). The final product distribution showed that the desired hetero-dual DA comprised 56% of the mixture, with **dCPT-Sup35** (31%) and **dPTX-Sup35** (13%) making up the remainder. The low conversion to **dPTX-Sup35** again clearly indicates that the bulky PTX causes steric hindrance during the directed disulphide exchange reaction. It should be noted that the two expected positional isomers of **CPT-PTX-Sup35** arising from the unsymmetrical nature of the bridging lysine residue could not be isolated from one another and 1H NMR analysis (Fig. S3 in ESI†) was unable to provide an accurate determination of the ratio.

Self-Assembly and Morphological Stability

Given that the bulky nature of PTX strongly influenced the product distribution during synthesis, we investigated the effect it could have on the self-assembly of the dual DAs under aqueous conditions. Solutions of all three dual DAs were prepared at 1 mM in water and allowed to age for 2 hours before diluting to 100 μM. Transmission electron microscopy (TEM) imaging and circular dichroism (CD) were recorded to evaluate the nanostructures formed and how they evolved over time (Fig. 2). All solutions were incubated at room temperature. Initially, the hetero-dual DA, **CPT-PTX-Sup35**, was observed to form two

†Electronic Supplementary Information (ESI) available: experimental procedures and protocols, molecular characterization, TEM, CD, fluorescence and release data. See DOI: 10.1039/b000000x/

types of filamentous nanostructures—small worm-like structures (7–8 nm widths), which display a strong tendency to curl up on themselves, and comparatively longer twisted filaments ~14 nm in width (Fig. 2a–b). If any β-sheet secondary structure is present, the CD analysis (Fig. 2f) indicates it is not predominant and is overwhelmed by the broad positive signal at 230 nm that can be attributed to PTX n–π* transitions.[59] The strong negative signal at 201 nm suggests that the peptide may be adopting either a random coil or poly-proline type-II-like structure.[63] Negative signals can also be observed for both PTX and CPT π–π* transitions, though PTX generally exhibits strong circular dichroism due to its three benzyl groups all being attached to asymmetric centres.[59] CPT on the other hand, exhibits stronger CD when in an aggregated state,[57] so the observation of a negative signal confirms that some degree of assembly is taking place.

After 24 h or longer incubation time, TEM imaging shows that the twisted filament morphology is the only nanostructure present and appears to have undergone significant growth to give contour lengths on the order of several μm (Fig. 2c–d). CD analysis indicates that the elongation is coincident with β-sheet formation, exhibiting the typical signal at 218 nm. The negative signals for the PTX and CPT π–π* transitions also undergo a blue-shift, suggesting a change in their surrounding environment. At the widest point, these fibrils are 13.9 ± 1.7 nm across, and at their narrowest appear to be approximately half of this value. These observations are thus suggestive of two entwined filaments, each of which is approximately 7 nm in width. Further aging does not appear to lead to any significant changes in the nanostructure, as indicated by TEM and CD analysis. Cryo-TEM imaging,[64] a technique that preserves the solution state structure in vitreous ice, confirms that long fibrous structures are obtained (Fig. 2e), however, the twisted nature could not be verified due to practical limitations of this technique.

The presence and morphologies of the two types of nanostructure in the initial stages bears remarkable similarity to the formation of amyloid fibrils[65] and filaments formed by peptidomimetics.[66] It has been proposed that amyloid fibrils rich in β-sheets assemble via a series of intermediate structures, beginning with narrow filaments that can twist around one another to give fibrils comprised of two or more filaments[67, 68] or undergo lateral associations to give a non-twisted ribbon-like assembly.[68, 69] Further changes can then occur to give twisted ribbons and tubes.[69] In our case, we observe the initial formation of short filaments that associate with one another to give two-filament fibrils. We propose that the short filaments are kinetically-favourable structures that result from the rapid hydrophobic collapse of **CPT-PTX-Sup35** molecules upon dissolution in water. The absence of the characteristic β-sheet absorption in the CD spectrum at early assembly stages indicates the elongation may not be directly linked to hydrogen bonding among Sup35 peptides, but rather as a result of molecular packing associated with the hydrophobic segments. It is very likely that a β-sheet is sterically hindered due to the mismatch in size between CPT and PTX. Given time, however, it appears that two of these filaments come together and by entwining can undergo reorganization of their internal structure, forming β-sheets that promote elongation of the fibrils to give the extended structures observed at later time points.

At this stage, we cannot rule out the influence that the two structural isomers of **CPT-PTX-Sup35** has on the self-assembly, however, the flexibility of the lysine side-chain and linkers should mitigate the potential mismatch between isomers that would occur on co-assembly. Furthermore, a small bisignate peak centred at 378 nm (one of the CPT π–π* transitions) in the CD spectrum hints at some potential CPT–CPT electronic interactions that may also play a role in the assembly process. Also, it is important to point out that, unlike the structural polymorphism shown by amyloid fibrils,[65] our data show that the two-filament fibrils are the end-point in the structural evolution, as no ribbon-like or other structures could be seen at any time point. We speculate that this may be a combination of the hydrophobic domain of **CPT-PTX-Sup35** being shielded from the aqueous environment (the amphiphilic nature of the designed DAs) and the fibril's twisted nature, with both properties preventing any further lateral associations that would give a ribbon-like morphology.

Further evidence for the evolution of the nanostructure from small filaments to twisted two-filament fibrils is provided by studying the effect of high salt concentration on the morphology. Dilution of the 1 mM stock solution of **CPT-PTX-Sup35** that had been aged for 2 h to 100 μM in Dulbecco's phosphate-buffered saline (1×DPBS) was seen to effectively retard the structural evolution, giving only the small filament morphology (Fig. 3a). Very little shift toward the twisted nanofilament structure was observed over the course of several days, with TEM analysis indicating only the smaller nanostructure with occasional examples of the entwined morphology (Fig. 3b). CD analysis confirms that there is a slow shift toward the β-sheet structure, though it does not reach the extent of the sample aged in water even after 3 days (Fig. S7a in ESI†). This slower rate of structural evolution may be due to increased shielding/crosslinking of the protonated lysine residues by the multivalent phosphate anions. Reorganization of the internal structure requires that the assembly be dynamic in nature, the extent of which would be greater in the absence of the phosphate ions. By providing a screening effect, the phosphate anions significantly reduce the rate at which reorganization can occur.

In contrast, dilution into 1×DPBS of a 1 mM sample (prepared in water) that had been allowed to age for 8 d exhibited both the same twisted fibril morphology (Fig. 3c) and CD spectrum observed in pure water (Fig. S7b in ESI†). This indicates that dilution into DPBS does not disrupt the nanostructures already present in solution and that the morphologies observed are true representations of the assemblies present in the stock solution. An interesting point to note is that inter-fibril bundling is not observed despite the increased charge shielding afforded by the phosphate ions, with the fibrils being observed only as single elements. This suggests that their twisted nature does indeed reduce the likelihood of further lateral associations.

In contrast to **CPT-PTX-Sup35**, the **dCPT-Sup35** homo-dual DA was found to rapidly form more typical filamentous structures, (Fig. 4a and Fig. S8 in ESI†) with a range of widths (5–15 nm). Closer inspection reveals that the wider structures are comprised of one or more narrower filaments (5.7 ± 2.4 nm) that associate with one another in no particularly defined manner, either running parallel or twisting about one another. CD analysis (Fig. 4c) shows a strong β-sheet signal at 218 nm that further intensifies upon aging. A slightly greater degree of filament bundling could also be seen at later time points (Fig. 4b).

The **dPTX-Sup35** homo-dual DA, on the other hand, was found to form predominantly spherical and short worm-like structures, even after longer incubation periods and at higher concentration (1 mM) (Fig. 4d–e). The dominant structures observed were small non-filamentous structures approximately 8 nm in width, similar in shape to those initially formed by **CPT-PTX-Sup35**. The typical PTX signals could be seen in the CD spectra—positive at 230 nm and negative at 255 and 295 nm—with no indication that any *β*-sheet secondary structure was present (Fig. 4f). It is clear from these observations that the two sterically demanding PTX molecules prevent neighbouring peptides from coming close enough to hydrogen bond with one another and form β-sheets. This also illustrates that while our branching methodology is an effective way to increase the drug loading of a DA, the nature of the drug being attached has the potential to alter the self-assembly process in an unexpected manner and must be taken into consideration when designing the conjugate.

The observations from this self-assembly study clearly demonstrate the effect that the PTX molecule can have when incorporated into a drug amphiphile. In its absence, the planar CPT can easily adopt a filamentous morphology, but the replacement of one CPT by the bulkier PTX results in a slower assembly process that ultimately gives a twisted fibrillar nanostructure. Replacement of both CPTs with PTX on the other hand leads to the formation

Physical Stability

To assess how the incorporation of the bulky PTX affects the stability of these nanostructures, we first examined the effect that dilution has upon the CD spectrum of the dual drug of only small micellar structures. conjugates. An aged sample of each conjugate (100 μM) was diluted 20-fold to 5 μM and the CD spectrum recorded immediately to determine if any change in the molecular packing had occurred (Fig. S9 in ESI[†]). For both **CPT-PTX-Sup35** and **dCPT-Sup35**, it can be seen that there is an immediate loss of the β-sheet signal that is suggestive of the dissociation of the respective nanostructures to smaller aggregates and/or single molecules. It should be noted that in our previous report,[38] the Tau peptide analogue of **dCPT-Sup35** was shown to have a stable nanostructure below even 1 μM, with the CD spectrum clearly indicating the presence of the *β*-sheet. That **dCPT-Sup35** appears to disassociate at low μM concentrations points to the important role that the peptide has in the overall self-assembly potential of the drug amphiphiles, with the hydrophilic Sup35 peptide (N_2Q_2NY) resulting in a nanostructure with an apparently higher critical aggregation concentration (CAC) than the more hydrophobic Tau peptide (VQIVY).

Next, we performed a Nile Red-based encapsulation study to quantify the CAC of **CPT-PTX-Sup35** and **dCPT-Sup35**. The emission spectrum of this solvatochromic fluorophore differs significantly when placed in hydrophobic or hydrophilic environments and thus can be used as a probe for assembly processes.[70, 71] Accordingly, various concentrations of **CPT-PTX-Sup35** or **dCPT-Sup35** were incubated overnight with 1 μM Nile Red before recording the emission spectra (exciting at 550 nm). Plotting the 640 nm emission data against the conjugate concentration gave CAC values between 20–30 μM for both DAs (Fig. S10 in ESI[†]), which fit into the CAC range reported by the Tirrell group for peptide amphiphile systems.[72] The response for **dCPT-Sup35** was found to be less than for **CPT-PTX-Sup35**, and is likely due to poor penetration of the dye into the assembly, which is

expected to have a high degree of internal order arising from the π-π stacking of the CPT units. The CAC of these DAs is determined by both the degree of hydrophobicity that they possess and the ease with which they can pack together. Given the similar values for the two DAs, it can be inferred that the greater hydrophobicity of PTX somewhat offsets the difficulty in packing that its incorporation introduces.

Hydrolytic Stability

Given the apparent effect that PTX incorporation has on the internal packing, we also performed hydrolytic stability experiments to probe how this affected the structural integrity of the studied DAs, using RP-HPLC to analyse 100 μM and 1 mM concentrations that had been allowed to age at room temperature for 2 weeks (Fig. S11 in ESI†). At 1 mM, both **dCPT-Sup35** and **CPT-PTX-Sup35** exhibited little degradation, whereas **dPTX-Sup35** showed significant breakdown of the conjugate. All three conjugates were found to undergo significant degradation at 100 μM, the relative extent of which leads us to conclude that the order of stability is **dCPT-Sup35 > CPT-PTX-Sup35 > dPTX-Sup35**. This is in agreement with PTX being a disruptive influence on the ordered molecular packing within the nanostructures. A more tightly packed structure will reduce access to the water-sensitive bonds that are located toward the centre of the assembly.

Drug Release

In order to evaluate the ability of **CPT-PTX-Sup35** to release its therapeutic cargo, we incubated a 50 μM solution of this dual DA at 37 °C in the presence or absence of the cancer-relevant reducing agent, glutathione (GSH) (Fig. 5a). Aliquots were taken at various time points, quenching the reaction by the addition of 1 M HCl and flash freezing in liquid nitrogen. These samples were then analysed by HPLC to determine the concentration of the important reaction components at each time point (**CPT-PTX-Sup35**, CPT and PTX). The conjugate was observed to degrade rapidly in the presence of GSH, being completely consumed within 2 h, whereas >80% remained after 8 h incubation in its absence. It can be seen that, initially at least, it is the linker-modified forms of the drugs that are released, namely **CPT-buSH** and **PTX-buSH**, which then undergo further hydrolysis to give the free drugs. Homo- and hetero-disulphide products, such as (**CPT-buS)$_2$**, **(PTX-buS)$_2$**, and **CPT-buS-Sbu-PTX**, can also be observed before they too undergo reduction and/or hydrolysis (Fig. 5b). Formation of these homo- and hetero-disulphide degradation products is likely a result of the supramolecular nature of the DA nanostructures, which leads to a high local concentration of released thiol products.[37] It can also be seen that unmodified PTX is released almost twice as fast as CPT in the presence of GSH, perhaps due to the PTX-ester bond being more labile than the CPT-ester bond—hydrolysis of a 2° alcohol ester (PTX) is expected to be faster than that of a 3° alcohol ester (CPT) due to steric considerations of the tetrahedral intermediate formed.

Cytotoxicity Study

The ability of **CPT-PTX-Sup35** to prohibit proliferation was assessed through the determination of a dose–response relationship against a PTX-resistant KB-V1 cervical cancer line (Fig. 6 and Fig. S12 in ESI†), incubating with **CPT-PTX-Sup35**, PTX, CPT or

dPTX-Sup35 for 48 h. It can be clearly seen that while free PTX or **dPTX-Sup35** do not exert any toxicity against the PTX-resistant cells (Fig. 6), the hetero dual drug conjugate, **CPT-PTX-Sup35**, can effectively kill a high proportion of the cell population, with an IC_{50} value of 194 nM. This activity is very similar to free CPT (Fig. S12 in ESI†) and clearly shows an advantage in having two different drugs delivered simultaneously, should the target prove to be resistant to one of cargo drugs. Against PTX-sensitive KB-3-1 cervical cancer cells, the activity of the hetero dual drug conjugate reflects that of free PTX with an IC_{50} value in the low nM range (Fig. S13 in ESI†). It should also be noted that the parent peptide, **dCys-Sup35**, exhibits no toxicity over the studied concentration range (Fig. S14 in ESI†) and as such does not contribute to the observed activity.

Discussion

The use of charged filamentous structures for systemic delivery is not yet an established technique owing to the potential for adsorption to proteins and even blockage of blood vessels as a result of aggregation. Soukasene *et al* have demonstrated that the encapsulation of CPT within peptide amphiphile nanofibers can be as effective as excipient-mediated delivery,[73] though it remains unknown what the fate of the nanofiber is during circulation and how the drug is ultimately released. Discher and co-workers have also shown that filomicellar structures can persist longer in circulation than their spherical counterparts,[74] though their length is a critical element that needs to be controlled. In order to utilize a system such as ours, it is essential that some control over the nanofilament's contour length is achieved. As currently presented, the combination of long contour length and low CMC value of **CPT-PTX-Sup35** would be problematic for systemic delivery. However, we envision that this filament-forming drug amphiphile can be adapted for local delivery applications.

Utilization of **CPT-PTX-Sup35** as a local drug delivery system would require further modification of the conjugate's physicochemical properties to promote gel formation. It is well known that filamentous nanostructures can be induced to form hydrogels through bundling and entanglement of individual filaments in response to screening of their surface charges. [7576] By appropriately modifying the peptide sequence of the dual drug amphiphile, this system could be induced to form a hydrogel that could then be applied directly to the tumour excision site to act as sustained release delivery vehicle, in a manner similar to that of the Gliadel® Wafer that is used to treat malignant glioma.[77] It is here that a higher CMC value relative to the drugs' low IC_{50} values will be of benefit, as the gel will serve as a reservoir for the drug conjugate, shedding individual molecules from the periphery that can then be degraded to release the free drug. Further tuning of the nanostructure properties can facilitate some degree of control over the release rate (a lower CMC would give a slower release rate, for instance). Delivering two drugs by this method may help to prevent tumour recurrence and avoid the development of multi-drug resistance.

Conclusions

In conclusion, we have demonstrated that the incorporation of two structurally distinct anticancer drug molecules into a single amphiphilic entity is a successful strategy for the creation of well-defined nanostructures. Combining CPT and PTX into a single hetero-dual

drug amphiphile was found to give nanostructures that possess a two-filament fibril morphology in which two narrower filaments entwine about one another. These results illustrate that the conjugation of two drugs with differing packing preferences onto one conjugate can be accomplished without compromising the self-assembly or chemotherapeutic properties. The advantage that delivering two drugs of completely different action mechanisms can have is the possibility for preventing the development of multi-drug resistance. The release of the more potent PTX will kill the majority of the cancer cells, with the remaining likely having developed some form of resistance. The presence of the second drug, CPT, to which they are not resistant, could then help to completely eliminate the cancerous cells and thus reduce the chances of recurrence.

Though this study presents one specific example, our future explorations of different drug combinations may allow us to establish some guiding principles that will allow us to rationally design the conjugates for particular nanostructures and even for specific applications. Additionally, the combination of two disparate hydrophobic moieties could represent a general strategy for the creation of entwined filamentous structures that, upon further entanglement to form hydrogels, could have interesting mechanical properties due to this close molecular level association. Furthermore, the grafting of two drugs with orthogonal mechanisms of action onto one conjugate would provide a means for gaining complete control over the drug ratio for potential combination therapy applications and promises benefits such as temporal and spatial control over release of the two bioactive agents for synergistic therapeutic effects. Ongoing efforts in our group are aiming to explore the potential that this approach has in the fields of self-assembly and drug delivery.

Experimental Section

Peptide synthesis

$(Ac\text{-}Cys)_2KGN_2Q_2NYK_2\text{-}NH_2$ (**dCys-Sup35**) was synthesized using a combination of automated (Focus XC automated peptide synthesizer, AAPPTEC, Louisville, KY, USA) and manual solid phase synthesis techniques, employing standard Fmoc chemistry protocols. Fmoc deprotections were performed using 20% 4-methylpiperidine in DMF and couplings were carried out using amino acid/HBTU/DIEA (4:3.98:6 relative to the resin) in DMF (with 2 min activation time). Acetylation was carried out manually using 20% acetic anhydride in DMF after *N*-terminal Fmoc deprotection. The branching lysine and terminal cysteines were introduced manually using Fmoc-Lys(Fmoc)-OH and HATU. The crude peptide was cleaved from the resin with a mixture containing trifluoroacetic acid, triisopropylsilane, water and ethane-1,2-dithiol in a ratio of 90:5:2.5:2.5 for 2 h, followed by trituration into cold diethyl ether. Purification was performed using RP-HPLC, and product fractions were identified by MALDI-Tof MS, combined and lyophilized to give **dCys-Sup35** as a white solid.

Dual Drug Amphiphile Synthesis

dCys-Sup35 (21 mg, 14 μmol) was dissolved in a solution of an N_2-purged DMSO containing a 1:1 mixture of **CPT-buSS-Pyr** (12 mg, 21 μmol) and **PTX-buSS-Pyr** (22.5 mg, 21 μmol) and allowed to react for 5 days. Analytical HPLC showed the reaction was

virtually complete, giving the expected doubly reacted products—**dCPT-Sup35**, **dPTX-Sup35** and **CPT-PTX-Sup35**. The reaction mixture was diluted to 10 mL with 0.1% TFA in acetonitrile/water (2:3) and purified by preparative RP-HPLC. The appropriate product fractions were combined and lyophilized. The powders obtained were then re-dissolved, calibrated and aliquotted into cryo-vials before re-lyophilization as described in the supporting information.

Transmission Electron Microscopy

Samples were prepared by depositing 7 μL of the appropriate solution onto a carbon-coated copper grid (Electron Microscopy Services, Hatfield, PA, USA), wicking away the excess solution with a small piece of filter paper. Next, 7 μL of a 2 wt % aqueous uranyl acetate solution was deposited and the excess solution was carefully removed as above to leave a very thin layer. The sample grid was then allowed to dry at room temperature prior to imaging. Bright-field TEM imaging was performed on a FEI Tecnai 12 TWIN Transmission Electron Microscope operated at an acceleration voltage of 100 kV. All TEM images were recorded by a SIS Megaview III wide-angle CCD camera.

Cryogenic Transmission Electron Microscopy

6 μL of sample solution was placed on a holey carbon film supported on a TEM copper grid (Electron Microscopy Services, Hatfield, PA, USA). All the TEM grids used for cryo-TEM imaging were treated with plasma air to render the lacey carbon film hydrophilic. A thin film of the sample solution was produced using a Vitrobot with controlled humidity chamber (FEI). After loading of the sample solution, the lacey carbon grid was blotted using preset parameters and plunged instantly into a liquid ethane reservoir pre-cooled by liquid nitrogen. The vitrified samples were then transferred to a cryo-holder and cryo-transfer stage that was cooled by liquid nitrogen. Imaging was performed using a FEI Tecnai 12 TWIN Transmission Electron Microscope (100 kV) and images were recorded by a 16 bit 2K × 2K FEI Eagle bottom mount camera. To prevent sublimation of vitreous water, the cryo-holder temperature was maintained below −170 °C during the imaging process.

Circular Dichroism

CD spectra were recorded on a Jasco J-710 spectropolarimeter (JASCO, Easton, MD, USA) using a 1 mm path length quartz UV-Vis absorption cell (Thermo Fisher Scientific, Pittsburgh, PA, USA). Background spectra of the solvents were acquired and subtracted from the sample spectra. Collected data was normalized with respect to sample concentration and number of β-sheet forming residues.

Drug Release Protocol

Briefly, a 100 μM solution **CPT-PTX-Sup35** in deionized water was freshly prepared and allowed to age for 24 h, before diluting to 50 μM with sodium phosphate buffer (pH 7.4, 20 mM) with or without GSH (20 mM) at the start of the experiment. The solutions were incubated at 37 °C and sampled at 0, 0.17, 0.5, 1, 2, 4, 6, and 8 h. The samples were acidified by the addition of 0.2 μL of 2 M HCl, flash frozen with liquid nitrogen and stored at −30 °C until HPLC could be performed. Immediately prior to the HPLC analysis, an

equal volume of DMSO was added to the sample to ensure complete dissolution of the reaction products (See S3 in SI for RP-HPLC conditions). The concentrations of **CPT-PTX-Sup35**, CPT and PTX were determined by measuring the area of the respective peaks in the HPLC chromatogram and comparing against a calibration curve for each species.

Cell Culture

KB-3-1 and KB-V1 cervical cancer cells were cultured in DMEM (Invitrogen) containing 10% fetal bovine serum (FBS, Invitrogen) and 1% of antibiotics (Invitrogen), and 1 μg/mL vinblastine was added for KB-V1 to maintain its multidrug resistance. The two cell types were incubated at 37 °C in an Oasis humidified incubator with a 5% CO_2 atmosphere (Caron, Marietta, OH).

Cytotoxicity Protocol

KB-V1 cells were seeded onto a 96-well plate (5×10^3 cells/well) and allowed to attach overnight. **PTX-CPT-Sup35** was diluted with fresh medium and incubated with cells immediately to achieve final conjugate concentrations of 0.01, 0.1, 1, 10, 100 and 1000 nM. Medium containing the same concentration of PTX or/and CPT in the form of free drugs were also used to incubate the cells, with non-treated cells (solvent only) as the control group. After 48 h incubation, the cell viability was determined using the SRB method according to the manufacturer's protocol (TOX-6, Sigma, St. Louis, MO).

Supplementary Material

Refer to Web version on PubMed Central for supplementary material.

Acknowledgments

This work was supported by the National Science Foundation (DMR 1255281), and National Institutes for Health training grants for A.G.C. (T-32CA130840) and Y.-A.L (R25CA153952). The authors thank the JHU Integrated Imaging Center (IIC) for the use of the TEM facility, and the JHU Department of Chemistry Mass Spectrometry facility. We also thank Prof. Kalina Hristova for the use of CD and fluorescence instru-mentation. KB-3-1 and KB-V1 cervical cancer cell lines were kindly provided by Dr. Gottesman (Center for Cancer Re-search, National Cancer Institute).

References

1. Aida T, Meijer EW, Stupp SI. Science. 2012; 335:813–817. [PubMed: 22344437]
2. Whitesides GM, Mathias JP, Seto CT. Science. 1991; 254:1312–1319. [PubMed: 1962191]
3. Iwaura R, Hoeben FJM, Masuda M, Schenning APHJ, Meijer EW, Shimizu T. J Am Chem Soc. 2006; 128:13298–13304. [PubMed: 17017812]
4. Thomas BN, Safinya CR, Plano RJ, Clark NA. Science. 1995; 267:1635–1638. [PubMed: 17808182]
5. Hirata H, Hattori N, Ishida M, Okabayashi H, Frusaka M, Zana R. J Phys Chem. 1995; 99:17778–17784.
6. Borse M, Sharma V, Aswal VK, Goyal PS, Devi S. J Colloid Interface Sci. 2005; 284:282–288. [PubMed: 15752815]
7. Rosenlehner K, Schade B, Boettcher C, Jaeger CM, Clark T, Heinemann FW, Hirsch A. Chem Eur J. 2010; 16:9544–9554. [PubMed: 20658504]

8. Schenning APHJ, Kilbinger AFM, Biscarini F, Cavallini M, Cooper HJ, Derrick PJ, Feast WJ, Lazzaroni R, Leclere P, McDonell LA, Meijer EW, Meskers SCJ. J Am Chem Soc. 2002; 124:1269–1275. [PubMed: 11841296]
9. Hamley IW. Biomacromolecules. 2014; 15:1543–1559. [PubMed: 24720400]
10. Kitamoto D, Morita T, Fukuoka T, Konishi M-a, Imura T. Curr Opin Colloid Interface Sci. 2009; 14:315–328.
11. Kuang Y, Gao Y, Shi JF, Li J, Xu B. Chemical Communications. 2014; 50:2772–2774. [PubMed: 24480853]
12. Ulijn RV, Smith AM. Chem Soc Rev. 2008; 37:664–675. [PubMed: 18362975]
13. Tu RS, Tirrell M. Adv Drug Delivery Rev. 2004; 56:1537–1563.
14. Gao Y, Berciu C, Kuang Y, Shi JF, Nicastro D, Xu B. ACS Nano. 2013; 7:9055–9063. [PubMed: 24067160]
15. Kuang Y, Xu B. Angew Chem, Int Ed. 2013; 52:6944–6948.
16. Debnath S, Roy S, Ulijn RV. Journal of the American Chemical Society. 2013; 135:16789–16792. [PubMed: 24147566]
17. Fleming S, Debnath S, Frederix P, Hunt NT, Ulijn RV. Biomacromolecules. 2014; 15:1171–1184. [PubMed: 24568678]
18. Middleton DA, Madine J, Castelletto V, Hamley IW. Angewandte Chemie-International Edition. 2013; 52:10537–10540.
19. Vernille JP, Kovell LC, Schneider JW. Bioconjugate Chem. 2004; 15:1314–1321.
20. Whitten DG, Chen LH, Geiger HC, Perlstein J, Song XD. J Phys Chem B. 1998; 102:10098–10111.
21. Henze O, Feast WJ, Gardebien F, Jonkheijm P, Lazzaroni R, Leclere P, Meijer EW, Schenning APHJ. J Am Chem Soc. 2006; 128:5923–5929. [PubMed: 16637660]
22. Tovar JD. Acc Chem Res. 2013; 46:1527–1537. [PubMed: 23477363]
23. Uhlenheuer DA, Petkau K, Brunsveld L. Chem Soc Rev. 2010; 39:2817–2826. [PubMed: 20461247]
24. Barnard A, Smith DK. Angew Chem, Int Ed. 2012; 51:6572–6581.
25. Petkau-Milroy K, Brunsveld L. Org Biomol Chem. 2013; 11:219–232. [PubMed: 23160566]
26. Jonker AM, Lowik D, van Hest JCM. Chem Mater. 2012; 24:759–773.
27. Levine PM, Carberry TP, Holub JM, Kirshenbaum K. MedChemComm. 2013; 4:493–509.
28. Duncan R. Nat Rev Cancer. 2006; 6:688–701. [PubMed: 16900224]
29. Yu Y, Chen CK, Law WC, Mok J, Zou J, Prasad PN, Cheng C. Mol Pharm. 2013; 10:867–874. [PubMed: 23181264]
30. Torchilin VP. Adv Drug Delivery Rev. 2012; 64:302–315.
31. Davis ME, Chen ZG, Shin DM. Nat Rev Drug Discov. 2008; 7:771–782. [PubMed: 18758474]
32. Reddy LH, Dubernet C, Mouelhi SL, Marque PE, Desmaele D, Couvreur P. J Controlled Release. 2007; 124:20–27.
33. Jin Y, Tong L, Ai P, Li M, Hou X. Int J Pharm. 2006; 309:199–207. [PubMed: 16377106]
34. Shen Y, Jin E, Zhang B, Murphy CJ, Sui M, Zhao J, Wang J, Tang J, Fan M, Van Kirk E, Murdoch WJ. J Am Chem Soc. 2010; 132:4259–4265. [PubMed: 20218672]
35. Li X-Q, Wen H-Y, Dong H-Q, Xue W-M, Pauletti GM, Cai X-J, Xia W-J, Shi D, Li Y-Y. Chem Commun. 2011; 47:8647–8649.
36. MacKay JA, Chen M, McDaniel JR, Liu W, Simnick AJ, Chilkoti A. Nat Mater. 2009; 8:993–997. [PubMed: 19898461]
37. Cheetham AG, Ou Y-C, Zhang P, Cui H. Chem Commun. 2014; 50:6039–6042.
38. Cheetham AG, Zhang P, Lin Y-A, Lock LL, Cui H. J Am Chem Soc. 2013; 135:2907–2910. [PubMed: 23379791]
39. Lin R, Cheetham AG, Zhang P, Lin Y-A, Cui H. Chem Commun. 2013; 49:4968–4970.
40. Gao Y, Kuang Y, Guo ZF, Guo ZH, Krauss IJ, Xu B. J Am Chem Soc. 2009; 131:13576–13577. [PubMed: 19731909]

41. Mao L, Wang H, Tan M, Ou L, Kong D, Yang Z. Chem Commun. 2012; 48:395–397.
42. Lock LL, LaComb M, Schwarz K, Cheetham AG, Lin YA, Zhang PC, Cui HG. Faraday Discuss. 2013; 166:285–301. [PubMed: 24611283]
43. Greco F, Vicent MJ. Adv Drug Delivery Rev. 2009; 61:1203–1213.
44. McDaniel JR, Bhattacharyya J, Vargo KB, Hassouneh W, Hammer DA, Chilkoti A. Angew Chem, Int Ed. 2013; 52:1683–1687.
45. Israelachvili, JN. Intermolecular and Surface Forces. Academic Press; San Diego: 2011.
46. Nagarajan R. Langmuir. 2001; 18:31–38.
47. Paramonov SE, Jun H-W, Hartgerink JD. J Am Chem Soc. 2006; 128:7291–7298. [PubMed: 16734483]
48. Balakrishnan K, Datar A, Naddo T, Huang J, Oitker R, Yen M, Zhao J, Zang L. J Am Chem Soc. 2006; 128:7390–7398. [PubMed: 16734495]
49. Banwell EF, Abelardo ES, Adams DJ, Birchall MA, Corrigan A, Donald AM, Kirkland M, Serpell LC, Butler MF, Woolfson DN. Nat Mater. 2009; 8:596–600. [PubMed: 19543314]
50. Bowerman CJ, Liyanage W, Federation AJ, Nilsson BL. Biomacromolecules. 2011; 12:2735–2745. [PubMed: 21568346]
51. Lundberg D, Faneca H, Moran MDC, Pedroso De Lima MC, Miguel MDG, Lindman B. Mol Membr Biol. 2011; 28:42–53. [PubMed: 21219253]
52. Pashuck ET, Cui H, Stupp SI. J Am Chem Soc. 2010; 132:6041–6046. [PubMed: 20377229]
53. Niece KL, Czeisler C, Sahni V, Tysseling-Mattiace V, Pashuck ET, Kessler JA, Stupp SI. Biomaterials. 2008; 29:4501–4509. [PubMed: 18774605]
54. Bakota EL, Sensoy O, Ozgur B, Sayar M, Hartgerink JD. Biomacromolecules. 2013; 14:1370–1378. [PubMed: 23480446]
55. Lin Y-A, Ou Y-C, Cheetham AG, Cui H. ACS Macro Letters. 2013; 2:1088–1094. [PubMed: 24490124]
56. Pommier Y. Nat Rev Cancer. 2006; 6:789–802. [PubMed: 16990856]
57. Nabiev I, Fleury F, Kudelina I, Pommier Y, Charton F, Riou JF, Alix AJP, Manfait M. Biochem Pharmacol. 1998; 55:1163–1174. [PubMed: 9719470]
58. Rowinsky EK, Donehower RC. N Engl J Med. 1995; 332:1004–1014. [PubMed: 7885406]
59. Balasubramanian SV, Alderfer JL, Straubinger RM. J Pharm Sci. 1994; 83:1470–1476. [PubMed: 7884672]
60. Jeansonne DP, Koh GY, Zhang F, Kirk-Ballard H, Wolff L, Liu D, Eilertsen K, Liu ZJ. Oncol Rep. 2011; 25:1473–1480. [PubMed: 21331447]
61. Dubikovskaya EA, Thorne SH, Pillow TH, Contag CH, Wender PA. Proc Natl Acad Sci U S A. 2008; 105:12128–12133. [PubMed: 18713866]
62. Nelson R, Sawaya MR, Balbirnie M, Madsen AO, Riekel C, Grothe R, Eisenberg D. Nature. 2005; 435:773–778. [PubMed: 15944695]
63. Makowska J, Rodziewicz-Motowidlo S, Baginska K, Vila JA, Liwo A, Chmurzynski L, Scheraga HA. Proc Natl Acad Sci U S A. 2006; 103:1744–1749. [PubMed: 16446433]
64. Danino D. Curr Opin Colloid Interface Sci. 2012; 17:316–329.
65. Fändrich M, Meinhardt J, Grigorieff N. Prion. 2009; 3:89–93. [PubMed: 19597329]
66. Lashuel HA, LaBrenz SR, Woo L, Serpell LC, Kelly JW. J Am Chem Soc. 2000; 122:5262–5277. [PubMed: 22339465]
67. Jimenez JL, Guijarro JI, Orlova E, Zurdo J, Dobson CM, Sunde M, Saibil HR. EMBO J. 1999; 18:815–821. [PubMed: 10022824]
68. Jiménez JL, Nettleton EJ, Bouchard M, Robinson CV, Dobson CM, Saibil HR. Proc Natl Acad Sci U S A. 2002; 99:9196–9201. [PubMed: 12093917]
69. Bauer HH, Aebi U, Häner M, Hermann R, Müller M, Arvinte T, Merkle HP. J Struct Biol. 1995; 115:1–15. [PubMed: 7577226]
70. Stuart MCA, van de Pas JC, Engberts JBFN. J Phys Org Chem. 2005; 18:929–934.
71. Lau C, Bitton R, Bianco-Peled H, Schultz DG, Cookson DJ, Grosser ST, Schneider JW. J Phys Chem B. 2006; 110:9027–9033. [PubMed: 16671711]

72. Missirlis D, Khant H, Tirrell M. Biochemistry. 2009; 48:3304–3314. [PubMed: 19245247]
73. Soukasene S, Toft DJ, Moyer TJ, Lu HM, Lee HK, Standley SM, Cryns VL, Stupp SI. ACS Nano. 2011; 5:9113–9121. [PubMed: 22044255]
74. Geng Y, Dalhaimer P, Cai S, Tsai R, Tewari M, Minko T, Discher DE. Nat Nanotechnol. 2007; 2:249–255. [PubMed: 18654271]
75. Cui HG, Webber MJ, Stupp SI. Biopolymers. 2010; 94:1–18. [PubMed: 20091874]
76. Du XW, Zhou J, Xu B. Chemistry-an Asian Journal. 2014; 9:1446–1472.
77. Perry J, Chambers A, Spithoff K, Laperriere N. Curr Oncol. 2007; 14:189–194. [PubMed: 17938702]

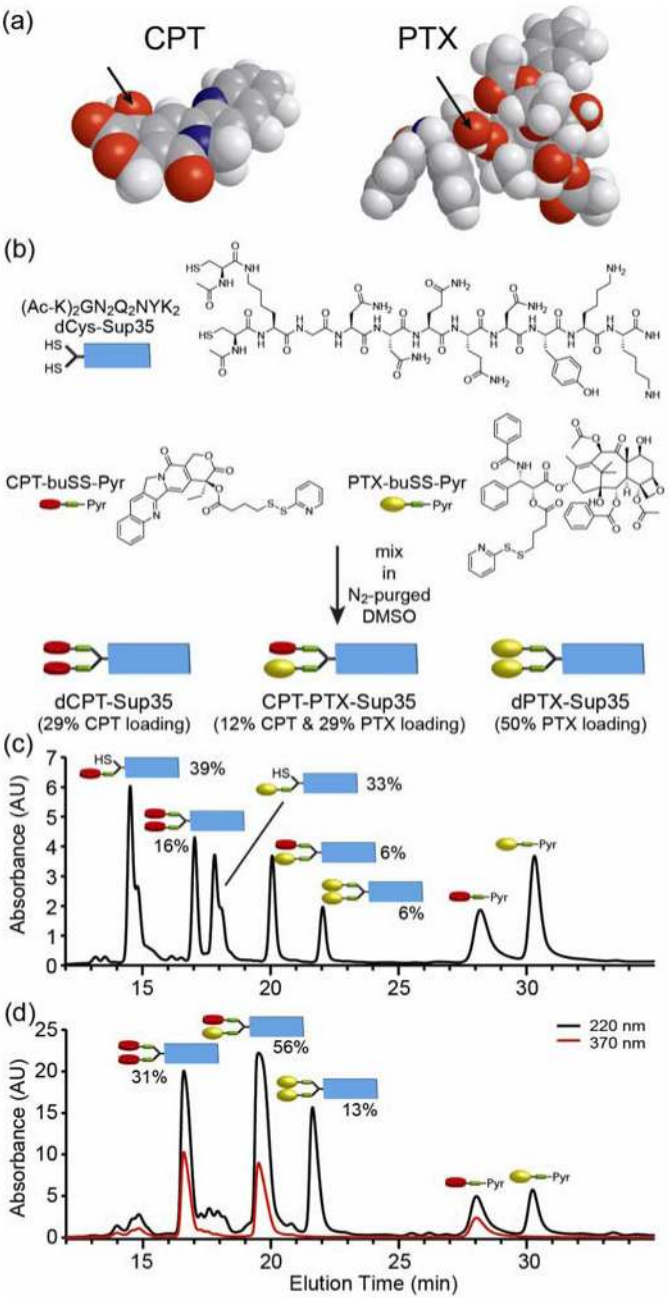

Fig. 1.

Effect of drug structure on the synthesis of the hetero-dual drug amphiphile (DA). Three-dimensional illustrations of the CPT and PTX structures, arrows indicate the conjugation point (a). Synthesis of **CPT-PTX-Sup35**, and homo-dual DAs, **dCPT-Sup35** and **dPTX-Sup35**, from the reaction of **dCys-Sup35** with a 1:1 mixture of activated disulphide drugs, **CPT-buSS-Pyr** and **PTX-buSS-Pyr** (b). Preparative HPLC chromatograms of the reaction of **dCys-Sup35** with (b) 1 equivalent of a 1:1 mixture of **CPT-buSS-Pyr** and **PTX-buSS-Pyr** after overnight reaction and (c) 3 equivalents of a 1:1 mixture of **CPT-buSS-Pyr** and **PTX-buSS-Pyr** after 5 days. Percentages give the relative amounts of the respective species

formed. The 220 nm traces (black) show absorptions from both CPT and PTX, whereas the 370 nm trace (red) corresponds to CPT absorptions only.

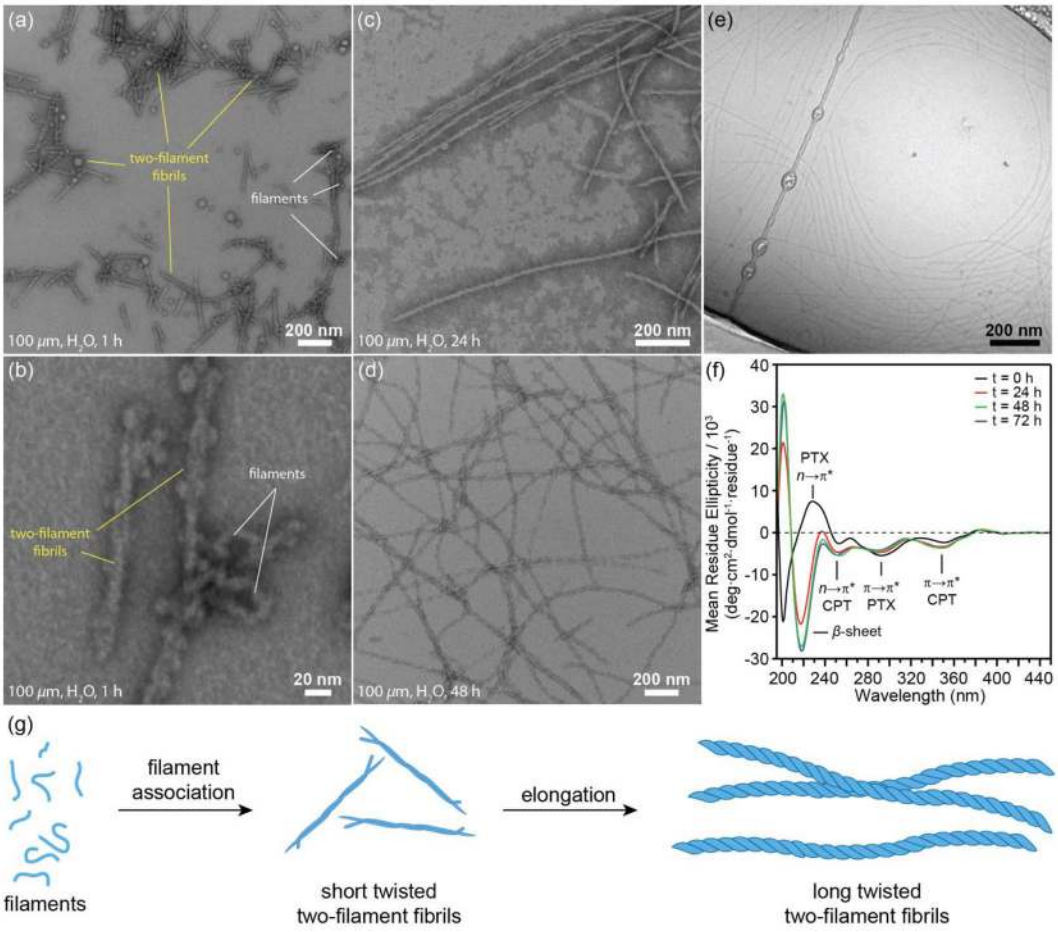

Fig. 2.

Self-assembly study of **CPT-PTX-Sup35**. Representative transmission electron microscopy (TEM) images of a 100 μM solution of **CPT-PTX-Sup35** in water 1 h (a and b), 24 h (c) and 48 h (d) after dilution of a 1 mM stock solution that had been allowed to age for 2 h. Cryo-TEM image of a 500 μM solution of **CPT-PTX-Sup35**, diluted from a 1 mM sample that had been aged for several days prior to sample preparation (e). Circular dichroism (CD) spectra of the 100 μM solution in water that was monitored over 3 days, showing the formation of the β-sheet secondary structure after 24 h incubation (f). TEM samples were negatively stained with 2 wt % uranyl acetate. Proposed mechanism for the formation of the long twisted twisted two-filament fibril structure (g).

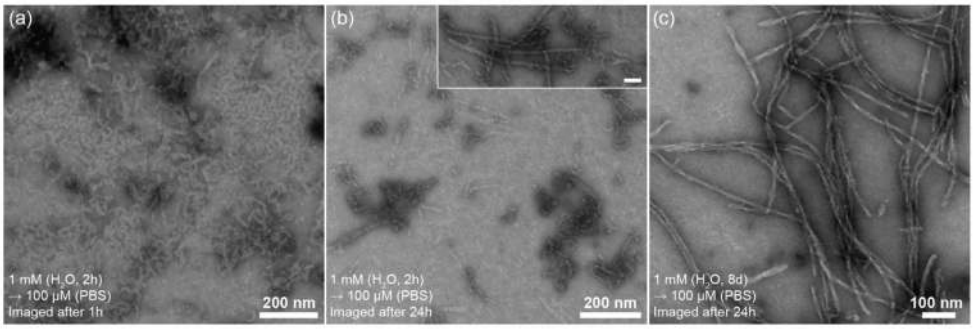

Fig. 3.

TEM images showing the effect of dilution into phosphate-buffered saline on the self-assembly of **CPT-PTX-Sup35**. Dilution of a 1 mM **CPT-PTX-Sup35** solution in H_2O after 2 h aging to give a 100 μM solution in PBS was found to significantly slow the formation of the twisted fibril morphology, essentially capturing the filament structures (a). After 24 h, little change was seen though twisted fibrils could be observed on occasion (b). In contrast, similar dilution of a 1 mM **CPT-PTX-Sup35** solution that had been allowed to age for 8 d gave only the twisted fibril structure, indicating that PBS does not affect the existing nanostructures.

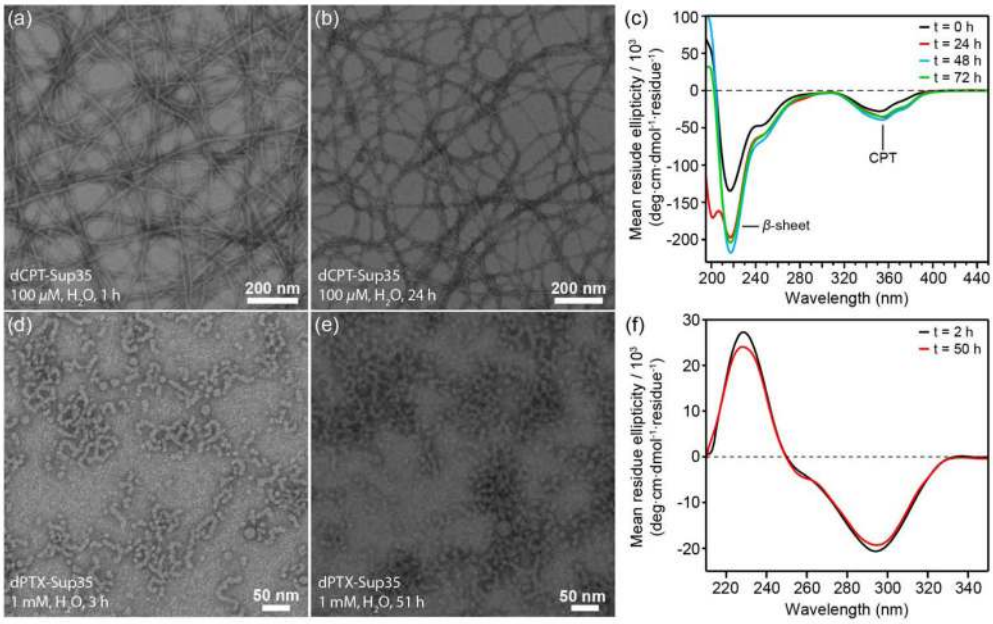

Fig. 4.

Self-assembly study of **dCPT-Sup35** and **dPTX-Sup35**. Representative TEM images of a 100 μM solution of **dCPT-Sup35** in H_2O 1 h (a) and 24 h (b) after dilution of a 1 mM stock solution that had been allowed to age for 2 h. CD analysis of the same 100 μM aqueous solution of **dCPT-Sup35** monitored over 3 days, showing the presence of the β-sheet secondary structure (c). The negative peak at 200 nm in the 24 h CD spectrum is an artifact produced by a HT value exceeding 800 V. Representative TEM images of a 1 mM solution of **dPTX-Sup35** in H_2O after 3 h (d) and 51 h aging (e). CD spectra of the same 1 mM aqueous solution of **dPTX-Sup35** at 2 h (black curve) and 50 h (red curve), indicating the absence of any β-sheet structure (f). Samples for analysis were diluted to 100 μM prior to measurement. TEM samples were negatively stained with 2 wt % uranyl acetate. The region below 210 nm for both concentrations was deemed unrepresentative due to HT values exceeding 800 V.

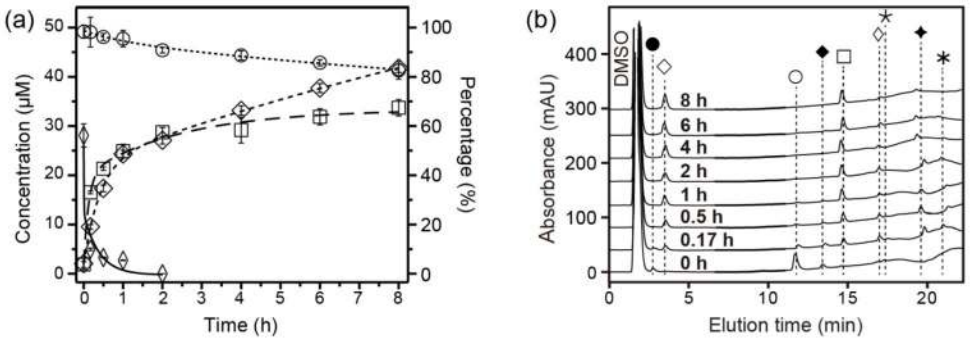

Fig. 5.

Drug release study. Release of CPT and PTX and degradation of CPT-PTX-Sup35 (50 μM in 10 mM sodium phosphate solution, pH 7.4, 37 °C) in the presence or absence of 10 mM GSH (○ CPT-PTX-Sup35 without GSH; ◊ CPT-PTX-Sup35 with GSH; ◇ released CPT; □ released PTX, all data are given as mean ± s.d. (n = 3) (a). HPLC chromatograms indicating the release products and intermediates at various time points (● CPT-GSH; ◆ CPT; ○ CPT-PTX-Sup35; ¿ CPT-buSH; □ PTX; ◊ $(CPT\text{-}buS)_2$; ⋆ PTX-buSH; ✦ CPT-buS-Sbu-PTX; ✳ $(PTX\text{-}buS)_2$) (b).

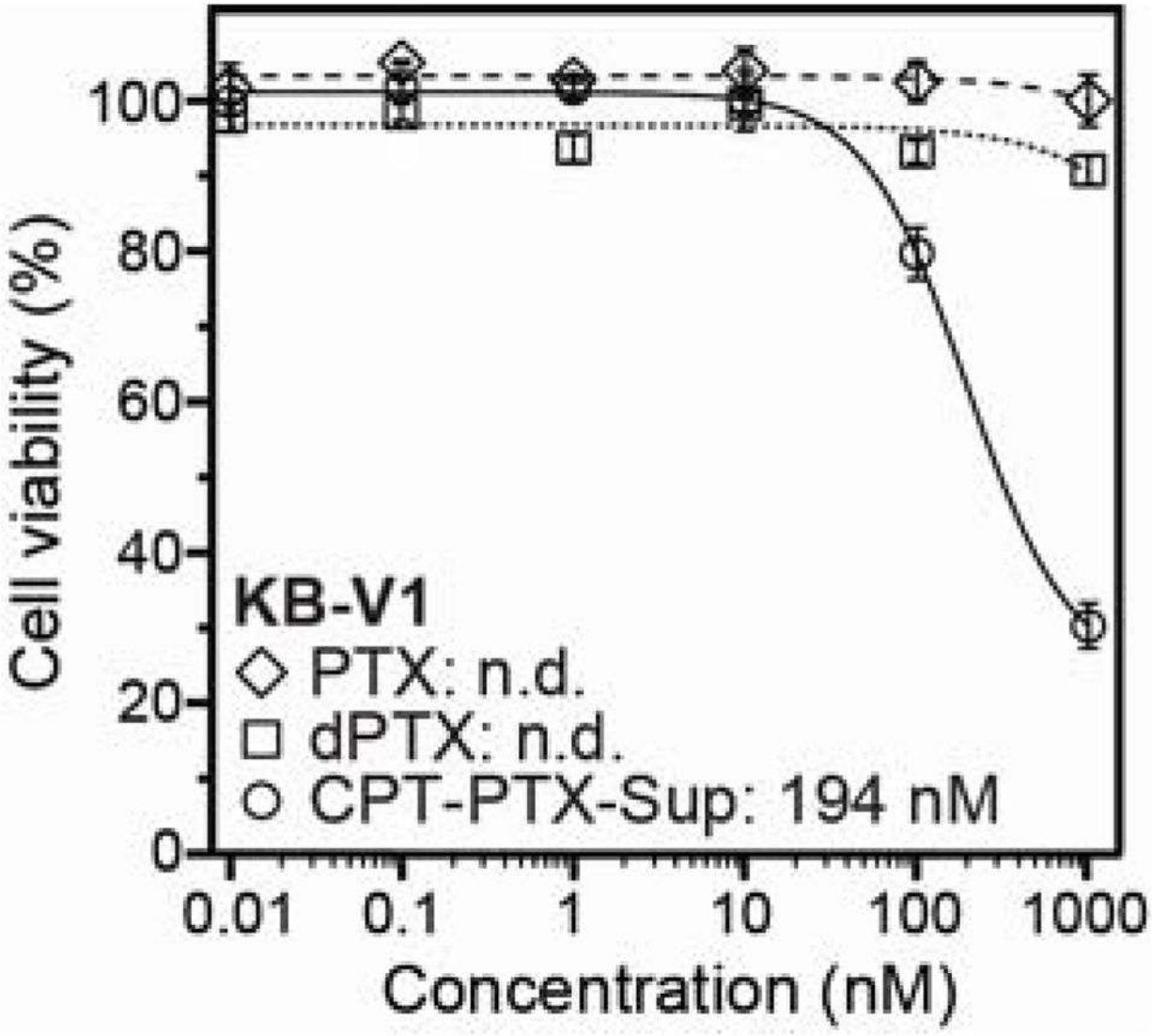

Fig. 6.

Cytotoxicity of **CPT-PTX-Sup35** against PTX-resistant KB-V1 cervical cancer cells (● **CPT-PTX-Sup35**; □ PTX; ◇ **dPTX-Sup35**). Cell viability was determined by SRB assay after 48 h incubation with the appropriate drug-containing media. Experiments were performed in triplicate and the mean values are plotted, standard deviations were less than 10%.